

RESEARCH

Open Access



Decreased protein activator of interferon induced protein kinase (PRKRA) involved in menopause-related cholesterol metabolic disorders by regulating cholesterol biosynthesis

Le Xu^{1,2}, Jian Xu³, Wanting Shi¹, Sa Zhang¹, Ting Guo^{1*} and Shien Zou^{1*}

Abstract

Background Menopause-related cholesterol metabolic disorders pose a global health concern, but the underlying mechanism is unclear. PRKRA was identified as a potential regulator of cholesterol metabolism in an exome-wide association study. Our prior research revealed a decrease in PRKRA expression in the ovarian cortex of postmenopausal women. However, its involvement in cholesterol metabolism disturbances in postmenopausal females remains unclear. This study aimed to investigate the association between PRKRA and cholesterol metabolism disorders in ovariectomized mice. Additionally, we elucidated the impact and underlying mechanisms of PRKRA on cholesterol metabolism in HepG2 and HuH7 cells.

Methods An ovariectomized mouse model was generated, and the mice were fed a standard diet for six months to simulate menopausal conditions. PRKRA expression in mouse liver tissue was evaluated by qPCR and western blotting. Spearman correlation analysis was used to explore the relationship between the PRKRA mRNA level and the serum total cholesterol concentration. In vitro, we investigated the influence of PRKRA on cholesterol levels and Dil-LDL uptake capacity in HepG2 and HuH7 cells. Additionally, transcriptome sequencing was employed to analyze the intrinsic mechanisms involved.

Results The ovariectomized mouse model exhibited abnormal lipid profiles that correlated with reduced PRKRA expression in the liver. In vitro, 17 β -estradiol (E₂) upregulated PRKRA expression, while follicle-stimulating hormone (FSH) downregulated it in HepG2 and HuH7 cells. PRKRA knockdown increased intracellular total cholesterol and decreased Dil-LDL uptake, while PRKRA overexpression had the opposite effects. Mechanistically, reduced PRKRA levels were associated with HMGCS1 upregulation and LDLR downregulation.

*Correspondence:

Ting Guo
drguoting@126.com
Shien Zou
zoushien@fudan.edu.cn

Full list of author information is available at the end of the article



© The Author(s) 2025. **Open Access** This article is licensed under a Creative Commons Attribution-NonCommercial-NoDerivatives 4.0 International License, which permits any non-commercial use, sharing, distribution and reproduction in any medium or format, as long as you give appropriate credit to the original author(s) and the source, provide a link to the Creative Commons licence, and indicate if you modified the licensed material. You do not have permission under this licence to share adapted material derived from this article or parts of it. The images or other third party material in this article are included in the article's Creative Commons licence, unless indicated otherwise in a credit line to the material. If material is not included in the article's Creative Commons licence and your intended use is not permitted by statutory regulation or exceeds the permitted use, you will need to obtain permission directly from the copyright holder. To view a copy of this licence, visit <http://creativecommons.org/licenses/by-nc-nd/4.0/>.

Conclusion Ovariectomy for six months independently induced an aberrant cholesterol phenotype in mice. Downregulation of PRKRA was implicated in cholesterol metabolism disturbances related to menopause, potentially through the regulation of cholesterol synthesis and LDL uptake.

Keywords Menopause, 17 β -estradiol, FSH, Cholesterol metabolism disorder, PRKRA

Introduction

Based on self-reported menstruation patterns, sexually mature females can be categorized into premenopausal, menopausal transition, and postmenopausal stages [1]. The juxtaposition of the increased average life expectancy resulting from the advancement of society with the unchanging age of menopause highlights the increasing significance of menopausal status in the overall trajectory of a woman's life. Menopause-related cholesterol metabolism disorders have emerged as prominent ailments that pose substantial threats to the well-being of women [2], including cardiovascular disease [3, 4], fatty liver disease [5], and hyperlipidemia [6].

The pivotal physiological alterations in postmenopausal women include decreased estrogen and increased FSH levels [7]. In recent years, considerable attention has been directed toward the roles of sex hormones, particularly estrogen and FSH, in menopause-related cholesterol metabolism disorders. However, the debate persisted regarding whether these hormones exert positive or negative regulatory effects, and the specific mechanism involved remained unclear. While some studies indicated that a decrease in estrogen levels was responsible for cholesterol metabolism disorders after menopause [8], others have presented contrasting evidence suggesting that estrogen may enhance cholesterol biosynthesis by stimulating the expression of sterol regulatory element-binding protein 2 (SREBP2), a crucial positive transcription factor in the cholesterol synthesis pathway [9]. In addition, several studies have suggested that elevated FSH contributes to this difference [10, 11]. Moreover, some research has shown that aging also plays a vital role in dyslipidemia [12, 13]. Menopausal status reflects complex physiological processes throughout a woman's lifespan characterized by changes not only in sex hormone levels but also at the molecular level [14]. Therefore, additional research is imperative to unravel the intricacies of this multifaceted issue.

The PRKRA gene encodes the protein activator of interferon-induced protein kinase (PACT), a protein activator of protein kinase R (PKR) [15] that responds to various cellular stress signals, including endoplasmic reticulum stress and oxidative stress [16]. In addition, PACT has been reported to be involved in cellular inflammatory responses [17], tumor formation [18], chemoresistance in mucinous ovarian cancer [19], and various other biological processes. A study in 2018 revealed that the antisense long noncoding RNA CHROME [20]

(the antisense strand of PRKRA, AC009948.5, CHROME, PRKRA-AS1) can regulate cholesterol homeostasis in primates. Furthermore, an exome-wide association study implicated PRKRA as a potential regulatory target in cholesterol metabolism [21]. Additionally, the Mouse Genome Informatics database indicated that knocking down PRKRA in mice results in the phenotype of elevated serum total cholesterol levels. However, no basic research has been reported in this domain to date. Moreover, our group has been committed to exploring the mechanisms of natural menopause and menopause-related disease [22], with PRKRA as one of our areas of focus. Therefore, in this study, we aimed to investigate whether PRKRA was involved in menopause-related cholesterol metabolism disorders, potentially by providing novel insights into this disease.

In this study, we used an ovariectomized mouse model and conducted in vitro experiments to evaluate the potential role of PRKRA in postmenopausal cholesterol metabolism disorders and to increase the understanding of the related regulatory pathways. Given the pivotal role of the liver in cholesterol metabolism, previous research has indicated that alterations in liver metabolism are among the initial events in obesity induced by ovariectomy [23, 24]. Therefore, our investigation specifically targeted hepatocytes.

Materials and methods

Animals and animal husbandry

We employed an ovariectomized mouse model (OVX) to investigate the impact of menopausal status on cholesterol metabolism. Female C57BL/6 mice aged 6–8 weeks were procured from Shanghai JSJ Laboratory Animal Co., Ltd. These mice were housed in a specific-pathogen-free (SPF) barrier environment in a temperature-controlled room (25 \pm 1 $^{\circ}$ C) with a 12 h light/12 h dark cycle and were acclimatized for one week.

Female C57BL/6 mice were randomly allocated to two groups: the sham group ($n=6$) and the OVX group ($n=6$). For the ovary removal surgery, 9-week-old female C57BL/6 mice were subjected to general anesthesia (tribromoethanol, 0.2 ml/10 g) and underwent either a sham operation or bilateral ovariectomy. Serum estrogen and FSH levels were monitored one week after surgery to confirm the success of the surgical procedure. Mice were sacrificed by cervical dislocation at 26 weeks (six months) after the surgery.

All the procedures were approved by the Animal Welfare and Ethics Group, Department of Laboratory Animal Science, Fudan University (Approval ID: 202311011Z).

ELISAs

ELISAs were used to quantify the serum E_2 and FSH levels in the mice to validate the success of the ovariectomy. Mouse serum samples were assessed using a Mouse Estradiol ELISA Kit (CUSABIO, CSB-e05109m) and a Mouse FSH ELISA Kit (CUSABIO, CSB-e06871m) to quantify E_2 and FSH levels, respectively. Approximately 200 μ l of blood was collected from the submandibular vein of each mouse one week after bilateral ovariectomy. Blood samples from the sham group were collected during the diestrus phase of the mouse estrous cycle to establish baseline estradiol levels. The procedural details closely adhered to the methodologies outlined in the manuscript.

Lipid profile measurements

Twenty-six weeks post-surgery, the mice were fasted overnight before blood collection. Following the intraperitoneal anesthesia of the mice, eyeball extraction was performed for blood sampling in the study. Subsequently, the samples were allowed to equilibrate at room temperature for 2 h, followed by centrifugation at 4 °C for 20 min at 3000 rpm. The resulting supernatant was then retrieved and either stored at -20 °C or subjected to immediate analysis. Lipid parameters, including total cholesterol (TC) (Rayto, S03042), triglyceride (TG) (Rayto, S03027), high-density lipoprotein cholesterol (HDL-C) (Rayto, S03025), low-density lipoprotein cholesterol (LDL-C) (Rayto, S03029), alanine aminotransferase (ALT) (Rayto, S03030), aspartate aminotransferase (AST) (Rayto, S03040) and alkaline phosphatase (ALP) (Rayto, S03038) were determined with the use of commercially available assay kits. An automatic biochemical analyzer (Rayto, Chemray 800) was used to assess blood lipid levels.

Hematoxylin and Eosin (HE) staining

Fixation: Liver tissue samples were dissected and washed with PBS (BasalMedia, B320KJ), followed by overnight fixation in 4% paraformaldehyde (Servicebio, G1101).

Paraffin Section Deparaffinization and Hydration: The paraffin sections were sequentially immersed in xylene I, xylene II, and xylene III for 10 min each, followed by absolute ethanol I and ethanol II for 5 min each. Gradient deparaffinization was performed with 90% ethanol, 80% ethanol, 70% ethanol, and 50% ethanol, each for 5 min each.

Hematoxylin and Eosin (HE) Staining: Paraffin sections were submerged in hematoxylin dye for 0.5–1 min, rinsed with tap water, briefly differentiated in 1% hydrochloric

acid alcohol, and then rinsed again. The sections were immersed in a 1% ammonia water solution for 1 min causing them to turn blue, which was then followed by a brief rinse under running water. The sections were then stained with eosin dye for a short duration and rinsed under running water.

Dehydration and Mounting: Paraffin sections were dehydrated by immersion in 75% ethanol for 2 min, 85% ethanol for 2 min, and absolute ethanol twice for 5 min each. Finally, the sections were immersed in xylene for 5 min to achieve transparency before mounting. The sections were removed from xylene and mounted with neutral gum.

Oil red O staining

The frozen tissue sections were restored to room temperature for 30 min. Subsequently, the sections were incubated with 60% (v/v) isopropanol for 2 min, followed by a 10-minute treatment with an Oil Red O working solution (consisting of 0.5% Oil Red O solution and ddH₂O at a 3:2 ratio). To achieve optimal staining, the slides were then subjected to a 5–10 s incubation with 60% (v/v) isopropanol, followed by a one-minute water wash. The nuclei were stained by incubation with hematoxylin for one minute, and differentiation was carried out using 1% hydrochloric acid alcohol for 5–10 s, followed by thorough washing in running water. Finally, the cells were observed under a microscope.

Quantitative polymerase chain reaction (qPCR)

Total RNA was isolated from cells using an EZ-press RNA Purification Kit (EZB, B0004DP), while total RNA was isolated from tissues by using the RNA Isolater Total RNA Extraction Reagent (Vazyme, R401, China) following the manufacturer's protocols. Then, cDNA was synthesized from 1 μ g of total RNA by using a Color Reverse Transcription Kit (EZB, A0010CGQ) following the manufacturer's guidelines. Then, qPCR was performed with 2 \times SYBR Green qPCR Master Mix (A0001) with a QUANTSTUDIO™ 3 and 5 Real-Time PCR instruments, and the results were analyzed using the 2^{- $\Delta\Delta$ Ct} method. The results were normalized to that of ACTB (β -actin). The experiments were repeated at least three times. The primer sequences used in the study are listed in the supplementary materials (Table S1).

Western blotting

Total protein was extracted from lysed cells or tissues using RIPA buffer supplemented with protease phosphatase inhibitors. Equal amounts of total protein were separated by 7.5–10% SDS-PAGE gels and transferred onto 0.22 μ m polyvinylidene fluoride (PVDF) membranes through electroblotting. Then, the membranes were incubated for 1 h at room temperature with 5%

nonfat milk in Tris-buffered saline containing Tween-20 (TBST) to block nonspecific binding. Next, the membranes were incubated overnight at 4 °C with primary antibodies, including anti-ACTB (1:1000; Servicebio, GB15003), anti-HMGCR (1:500; Affinity, DF6518), anti-HMGCS1 (1:1000; Proteintech, 17643-1-AP), anti-LDLR (1:1500; Proteintech, 10785-1-AP), anti-PCSK9 (1:1000; Affinity, DF12687), and anti-PRKRA (1:1000; Abcam, ab75749). Afterward, the membranes were washed three times with TBST for 10 min each. Then, the membranes were incubated with the corresponding secondary antibodies (1:3000; Abcam, ab6721) for 1 h at room temperature. Immune complexes were detected using enhanced chemiluminescence reagents (Millipore), and grayscale analysis was conducted using ImageJ.

Cell culture and treatment

HepG2 and HuH7 cells were obtained from the Stem Cell Bank, Chinese Academy of Sciences. The two cell lines were cultured in Dulbecco's modified Eagle's medium (DMEM) lacking phenol red (BasalMedia, China, L140KJ) and supplemented with 10% fetal bovine serum (FBS; Gibco, USA, C0232), 100 IU/ml penicillin and 100 µg/ml streptomycin (Gibco, USA, 15140122) at 37 °C in an atmosphere of 5% CO₂. During functional experiments, the normal FBS was replaced with certified Charcoal-stripped FBS (BI, Israel, 04-201-1 A, BI) to remove or reduce hormones, steroids, and other biologically active substances from the serum.

Drug treatment: HepG2 (5×10^5 /well) or HuH7 (2×10^5 /well) cells were seeded in 6-well plates until 50–60% confluence. Subsequently, the cells were starved in phenol red-free DMEM medium supplemented with 0.1% charcoal-stripped fetal bovine serum for 12–16 h, followed by treatment with 10% charcoal-stripped phenol red-free DMEM medium containing different concentrations of estradiol (Sigma-Aldrich, USA, E8875) or FSH (ProSpec, Israel, HOR-253) for 48 h. The drugs were dissolved and stored according to the instructions.

Small interfering RNA (siRNA) transfection

Three different PRKRA siRNAs and negative control siRNAs were purchased from Guangzhou Ribo. The sequences used were as follows: si-1, GTAAGAAGCTG GCGAAACA; si-2, GGACATTCCTTTAGGATGTA; and si-3, GCTAGAGTCATTTATGGAA. HepG2 (5×10^5 /well) and HuH7 (2×10^5 /well) cells were seeded into 6-well plates, and upon reaching 50–60% confluence, the cells were transfected with siRNA (50 nM) using Lipofectamine 3000 (Thermo Fisher Scientific, L3000015) following the manufacturer's instructions. RNA and proteins were extracted 48 and 72 h after transfection, respectively. The siRNAs with a silencing efficacy of more than 70% were selected for further experiments.

PRKRA lentivirus transfection

A stable PRKRA overexpression lentivirus was produced by GenePharma (Shanghai, China). HuH7 cells were seeded in a 6-well plate (75000 cells/well) one day before transfection. Transfection was conducted within 24 h using a lentiviral vector designed for the overexpression of PRKRA and its control, with the multiplicity of infection (MOI) set at 10. After 16–18 h of transfection, the medium was changed. After 3 days of transfection, the cells were subjected to selection pressure via puromycin (1.5 µg/ml) for 7 days to isolate stably transfected cells. Transfection efficiency was assessed one week postselection using quantitative PCR and western blotting.

Intracellular TC assay

The level of intracellular total cholesterol was determined using a Cholesterol Assay Kit (Applygen Technologies, E1015, Beijing, China) according to the manufacturer's instructions, and the cholesterol concentration was normalized to the protein concentration. The experiments were conducted at least three times.

Dil-LDL assay

Human Dil-LDL (Yuan, YB0011, China), labeled with the fluorescent probe Dil (1,1'-dioctadecyl-3,3',3'-tetramethyl-indocarbocyanine perchlorate), was used to assess the impact of the various treatments on the ability of HepG2 and HuH7 cells to internalize LDL, providing insights into the cellular mechanisms involved in LDL uptake under different conditions. The outcomes of this study will contribute to enhancing our understanding of the factors influencing cellular LDL absorption and, by extension, the potential impact on liver-mediated LDL clearance [25]. HepG2 and HuH7 cells were subjected to various treatments, and after each treatment, the culture medium was discarded. Subsequently, the cells were incubated with a medium containing 10 µg/ml fluorescent Dil-LDL for 2 h at 37 °C in the absence of light. After another three washes with PBS, the DAPI staining solution was applied for 5 min, followed by a final round of washing. The cells were observed using a fluorescence microscope. The experiments were performed in triplicate. The average fluorescence intensity was quantified using ImageJ software.

RNA sequencing

Transcriptomic analyses were also conducted to elucidate the potential molecular mechanisms involved. HepG2 cells were transfected with either si-NC or the most efficacious siRNA, si-PRKRA1, for 48 h. Total RNA was subsequently extracted using RNA isolation Total RNA Extraction Reagent (R401-01) according to the manufacturer's instructions. The experiment was independently performed three times to generate biological replicates.

A NanoDrop 2000 spectrophotometer (Thermo Scientific, USA) was used to evaluate RNA purity and quantity. The RNA integrity, for which the requisite RNA integrity number (RIN) for the construction of RNA-seq libraries should exceed 7, was evaluated using an Agilent 2100 Bioanalyzer (Agilent Technologies, Santa Clara, CA, USA). The VAHTS Universal V6 RNA-seq Library Prep Kit was used to construct libraries according to the manufacturer's instructions. The libraries were sequenced on the Illumina NovaSeq 6000 platform, and 150 bp paired-end reads were generated. Transcriptome sequencing and analysis were subsequently conducted by OE Biotech Co., Ltd. (Shanghai, China).

Differentially expressed genes (DEGs) were then identified utilizing the DESeq2 package, with significance defined as a p -value less than 0.05 and a fold change exceeding 1.5 (upregulation) or less than 0.5 (downregulation). Gene Ontology (GO) and Kyoto Encyclopedia of Genes and Genomes (KEGG) pathway enrichment analyses were performed for the identified DEGs. Gene set enrichment analysis (GSEA) was performed with GSEA software (<http://www.broadinstitute.org/gsea>) under the following filter conditions: $|\text{NES}| > 1$, $p < 0.05$, and $\text{FDR} < 0.25$.

Cell counting Kit-8 (CCK8) assay

The CCK-8 assay (New Cell & Molecular Biotech, Suzhou, China) was utilized to evaluate the toxicity of 17β -estradiol at various concentrations in HepG2 cells. HepG2 cells were cultivated in 96-well plates at a density of approximately 10,000 cells/well in 100 μL of medium, and treated with different estrogen concentrations for 48 h. After incubation, the medium was exchanged. Then, 110 μL of medium containing 10 μL of CCK8 solution was added to each well and allowed to incubate for 1 h. The absorbance at 450 nm was determined using a microplate reader. All the experiments were repeated in triplicate.

Statistical analysis

Continuous parametric variables are shown as the mean \pm standard error. Student's t -tests were performed to analyze the differences between the two groups, while one-way ANOVA was employed to evaluate the significant differences among more than two groups. Correlation analysis was conducted using Spearman's rank correlation analysis. A two-tailed P value less than 0.05 indicated statistical significance. The analyses were performed using GraphPad Prism version 9.

Results

OVX mice exhibited abnormal lipid profiles

To explore the mechanisms underlying menopause-related cholesterol metabolism disorders, we initially established a mouse model by ovariectomy to simulate

the menopausal state. Previous studies often induced postmenopausal cholesterol metabolism disorders by combining ovariectomy with a high-fat, high-cholesterol diet. In this study, we extended the modeling duration and continued feeding for 6 months with standard feed to investigate the independent impact of ovariectomy on systemic cholesterol metabolism. The flowchart for the animal experiments is shown in Fig. 1A.

Successful establishment of the menopausal model was confirmed by the observation of genital organ atrophy, low serum E_2 levels, and elevated FSH levels, as depicted in Fig. 1B and C. Compared to the sham group mice, the OVX mice exhibited a decrease in the liver weight/body weight, although there was no statistically significant difference in the total liver weight between the two groups (Fig. 1D). HE and Oil Red O staining of liver tissues revealed greater accumulation of lipid droplets in the OVX group (Fig. 1E). Furthermore, at 26 weeks post-surgery, the OVX group mice displayed abnormal serum lipid profiles with significant increases in serum TC, LDL-C, HDL-C, and TG levels (Fig. 1F), while ALT, AST, and ALP levels did not significantly differ between the two groups (Fig. 1G).

In addition, we utilized qPCR to assess the expression of key mRNA molecules involved in cholesterol synthesis metabolism in mouse liver tissues. The results revealed that ovariectomy-induced cholesterol metabolism disorders in mouse liver tissues were characterized by an elevation in synthetic metabolism (Fig. 1H).

In summary, ovariectomy can independently induce cholesterol metabolism disorders in mice. Specifically, six months postsurgery, mice exhibited elevated TC, LDL-C, HDL-C, and TG levels, and increased accumulation of lipid droplets in the liver, which was indicative of fatty degeneration. Additionally, the mRNA expression levels of genes involved in hepatic cholesterol synthesis metabolism were upregulated. The serum and liver lipid profile alterations observed reflected the impact of menopause on cholesterol metabolism.

OVX repressed the hepatic expression of PRKRA

To investigate the potential regulatory role of PRKRA in menopausal-related cholesterol metabolism disorders, we characterized the mRNA and protein expression profiles of PRKRA in mouse liver tissues before and after ovariectomy by qPCR and western blotting and conducted a correlation analysis with serum total cholesterol levels.

Our data indicated consistent decreases in the PRKRA mRNA and protein expression levels, as illustrated in Fig. 2A and B. More importantly, there was a negative correlation ($r = -0.711$, $p = 0.0118$) between the level of PRKRA mRNA in mouse liver tissue and the serum total cholesterol level (Fig. 2C).

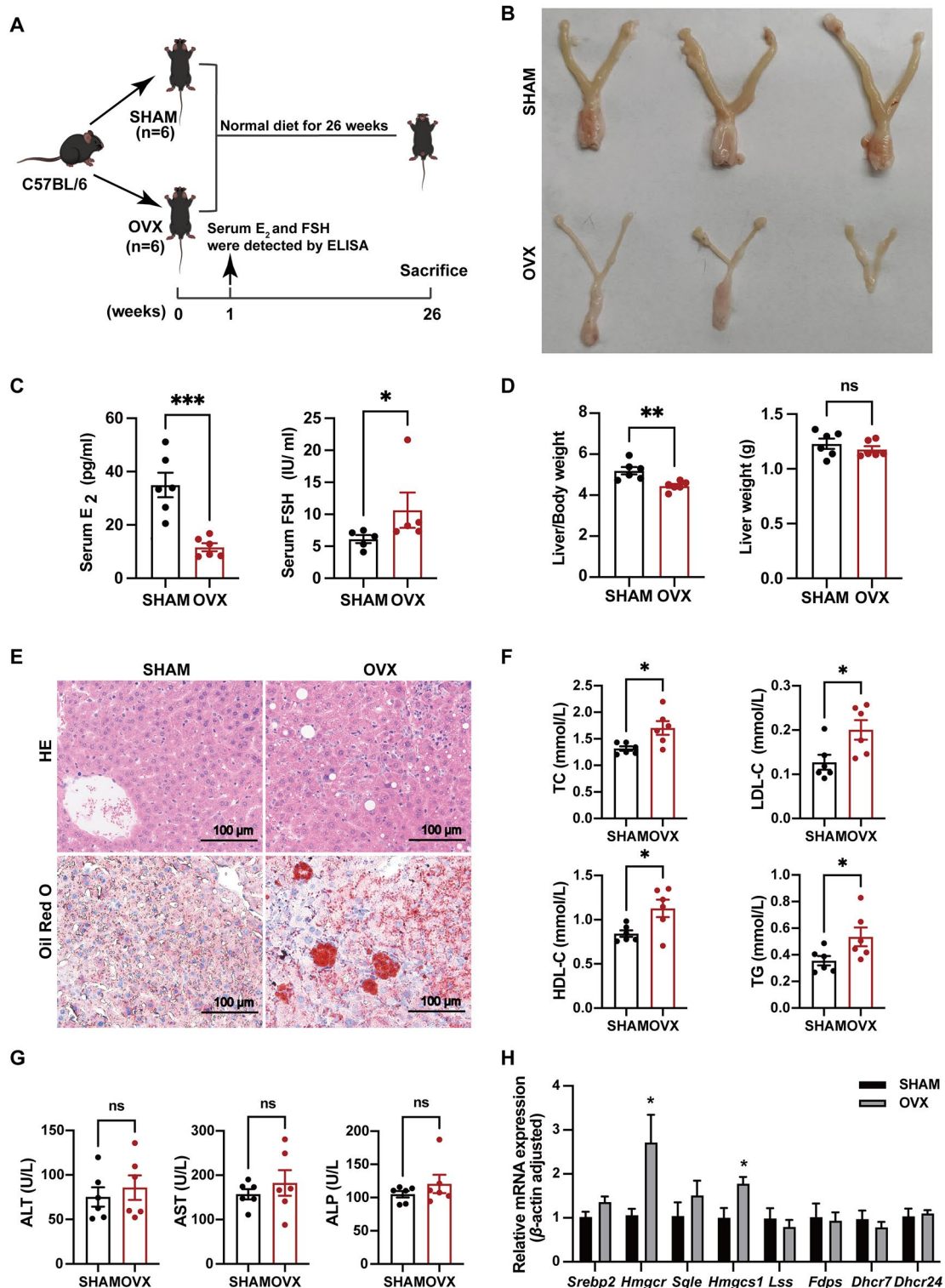


Fig. 1 OVX-induced lipid metabolism disruption in mice. **(A)** The flowchart for the animal experiments. **(B)** Uteri of mice in the sham and OVX groups. **(C)** The serum estradiol (E₂) and follicle-stimulating hormone (FSH) levels were measured 1 week after surgery in the sham (n=6) and OVX (n=6) groups. **(D)** Liver weights and liver/body weights of mice in the sham (n=6) and OVX (n=6) groups were measured 26 weeks after the surgery. **(E)** HE and Oil Red O staining of the liver; scale bar = 100 μm. **(F)** The serum levels of total cholesterol (TC), low-density lipoprotein cholesterol (LDL-C), high-density lipoprotein cholesterol (HDL-C), and triglycerides (TG) were measured 26 weeks after surgery in the sham (n=6) and OVX (n=6) groups. **(G)** The serum levels of alanine aminotransferase (ALT), aspartate aminotransferase (AST), and ALP. **(H)** The mRNA expression levels of key genes involved in cholesterol metabolism in the mouse liver were detected by qPCR. The data are shown as the mean ± SEM. Statistical significance is denoted as *P < 0.05, **P < 0.01, and ***P < 0.001; ns, not significant

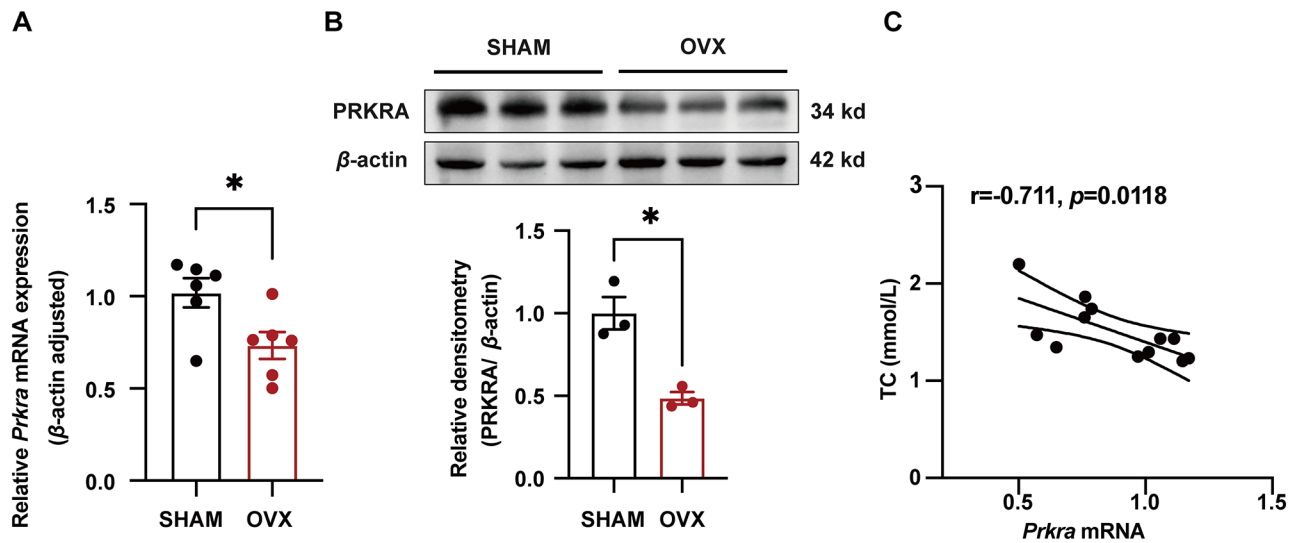


Fig. 2 OVX repressed hepatic expression of PRKRA. **(A)** The mRNA expression levels of PRKRA in the sham ($n=6$) and the OVX ($n=6$) groups. **(B)** PRKRA protein expression levels in the sham ($n=3$) and OVX ($n=3$) groups were assessed by western blotting. **(C)** The correlation between total cholesterol (TC) and PRKRA mRNA expression. * $P < 0.05$, ** $P < 0.01$

The above results indicated that PRKRA may be involved in ovariectomy-induced cholesterol metabolism disorders.

PRKRA expression was regulated by E_2 /FSH in HepG2 and HuH7 cells

Given the crucial role of hormonal fluctuations in the disruption of postmenopausal cholesterol metabolism, we conducted an in-depth investigation into whether PRKRA was regulated by sex hormones. This finding may provide an alternative perspective, suggesting the potential involvement of PRKRA in postmenopausal cholesterol metabolism disruption.

Initially, we employed the CCK8 assay to evaluate the potentially toxic effects of E_2 on HepG2 cells. Treatment with E_2 at concentrations less than 1000 nM had no significant impact on HepG2 cell viability (Fig. 3A). Building upon previous studies [26, 27], we employed three low doses of E_2 for subsequent experiments. The concentrations of FSH used were selected based on previous literature [10].

Our findings showed that E_2 effectively reduced intracellular TC levels, while FSH increased TC levels both in HepG2 (Fig. 3B) and HuH7 cells (Fig. 3C).

To explore the regulatory effect of E_2 and FSH on PRKRA expression, HepG2 and HuH7 cells were treated with varying concentrations of E_2 (1, 10, and 100 nM) and FSH (0, 2 and 10 ng/ml) for 48 h. Following treatment, we extracted total RNA and protein for expression analyses. Our results revealed that E_2 significantly increased both the PRKRA mRNA levels (Fig. 3D and E) and protein (Fig. 3F and G) expression levels. In contrast, FSH suppressed PRKRA expression (Fig. 3D and G).

PRKRA knockdown resulted in increased intracellular cholesterol levels and reduced LDL uptake

To assess the impact of PRKRA on hepatic cholesterol metabolism, three siRNAs were designed to specifically silence PRKRA expression. HepG2 and HuH7 cells were transfected with the designed PRKRA siRNAs. As depicted in Fig. 4A and B, successful knockdown of PRKRA expression was observed in both HepG2 and HuH7 cells at both the mRNA and protein levels.

Corresponding to the abnormal lipid profile observed in the OVX group mice, i.e., elevated serum TC and elevated LDL-C levels, we assessed the intracellular TC levels and the ability of cells to absorb LDL from the medium after PRKRA knockdown in vitro. When PRKRA was knocked down, the level of intracellular TC (Fig. 4C and E) increased, and LDL uptake (Fig. 4D and F) decreased in both HepG2 and HuH7 cells.

PRKRA expression is involved in the cholesterol biosynthesis pathway according to RNA-seq

To unravel the intricate underlying mechanisms and identify specific genes involved in cholesterol metabolism that change in response to PRKRA knockdown, we conducted RNA transcriptome sequencing (RNA-seq). Given the superior silencing efficiency of si-1, HepG2 cells were transfected with si-1 for 48 h, after which total RNA was extracted and subsequently subjected to transcriptome sequencing.

Differential expression analysis revealed a total of 209 DEGs in the si-NC vs. si-1 comparison, with 105 upregulated genes and 104 downregulated genes (Fig. 5A). Figure 5B showed the gene expression profiles between the two groups. A bubble chart constructed from the

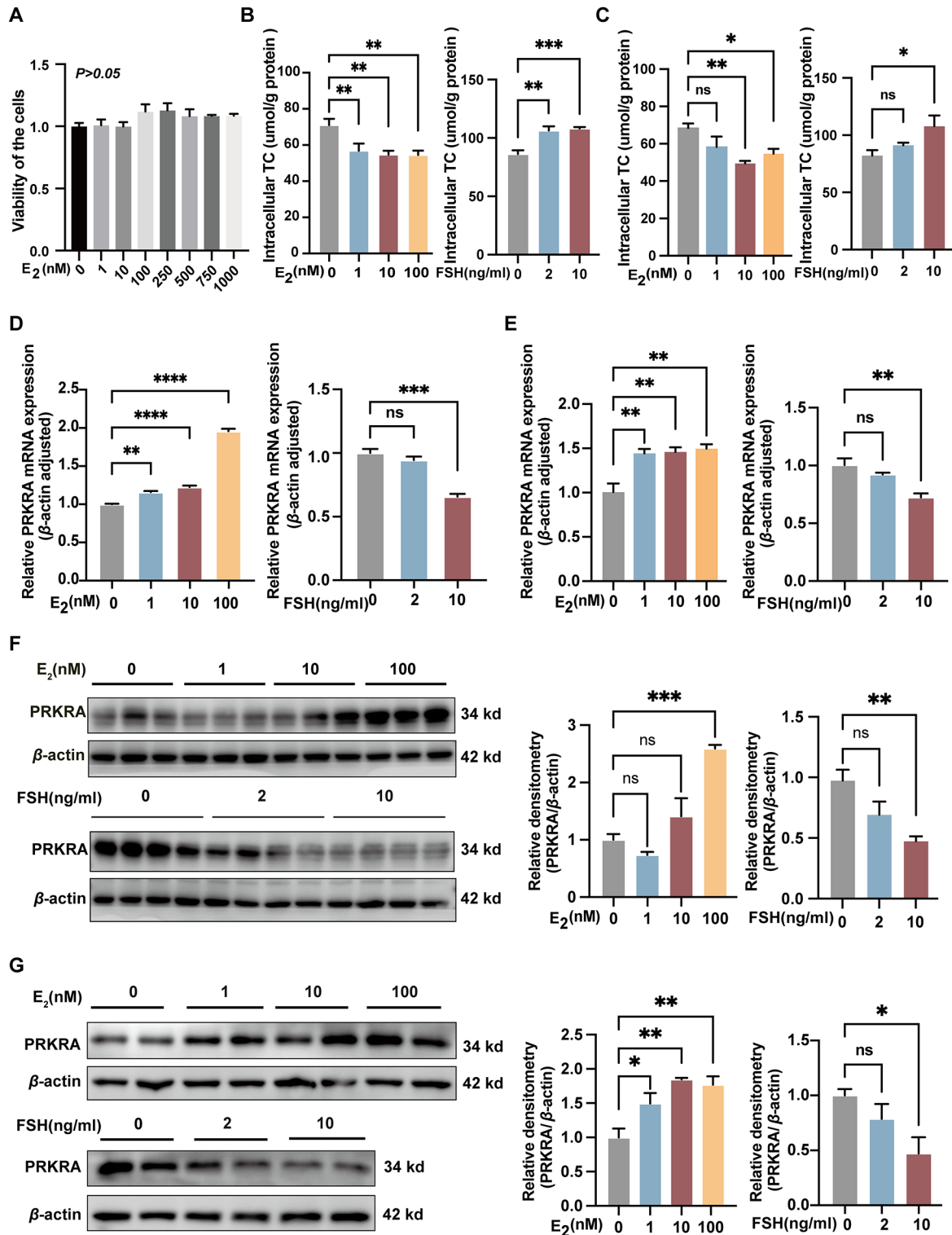


Fig. 3 FSH and E₂ regulated PRKRA expression. **(A)** CCK-8 assay results showing the effects of different concentrations of E₂ on cell proliferation and viability in HepG2 cells. **(B-C)** E₂ decreased the intracellular total cholesterol content, while FSH increased it. **(B):** HepG2 cells, **(C):** HuH7 cells. **(D-E)** E₂ increased the PRKRA mRNA expression, while FSH decreased it in HepG2 **(D)** and HuH7 cells **(E)**. **(F-G)** Treatment with E₂ increased PRKRA protein expression, and FSH decreased PRKRA protein expression. **(F):** HepG2 cells, **(G):** HuH7 cells. The histogram shows the mean ± SEM (*n* = 3) of separate experiments for each group. Statistical significance is indicated by **P* < 0.05, ***P* < 0.01, ****P* < 0.001, and *****P* < 0.0001; ns, not significant

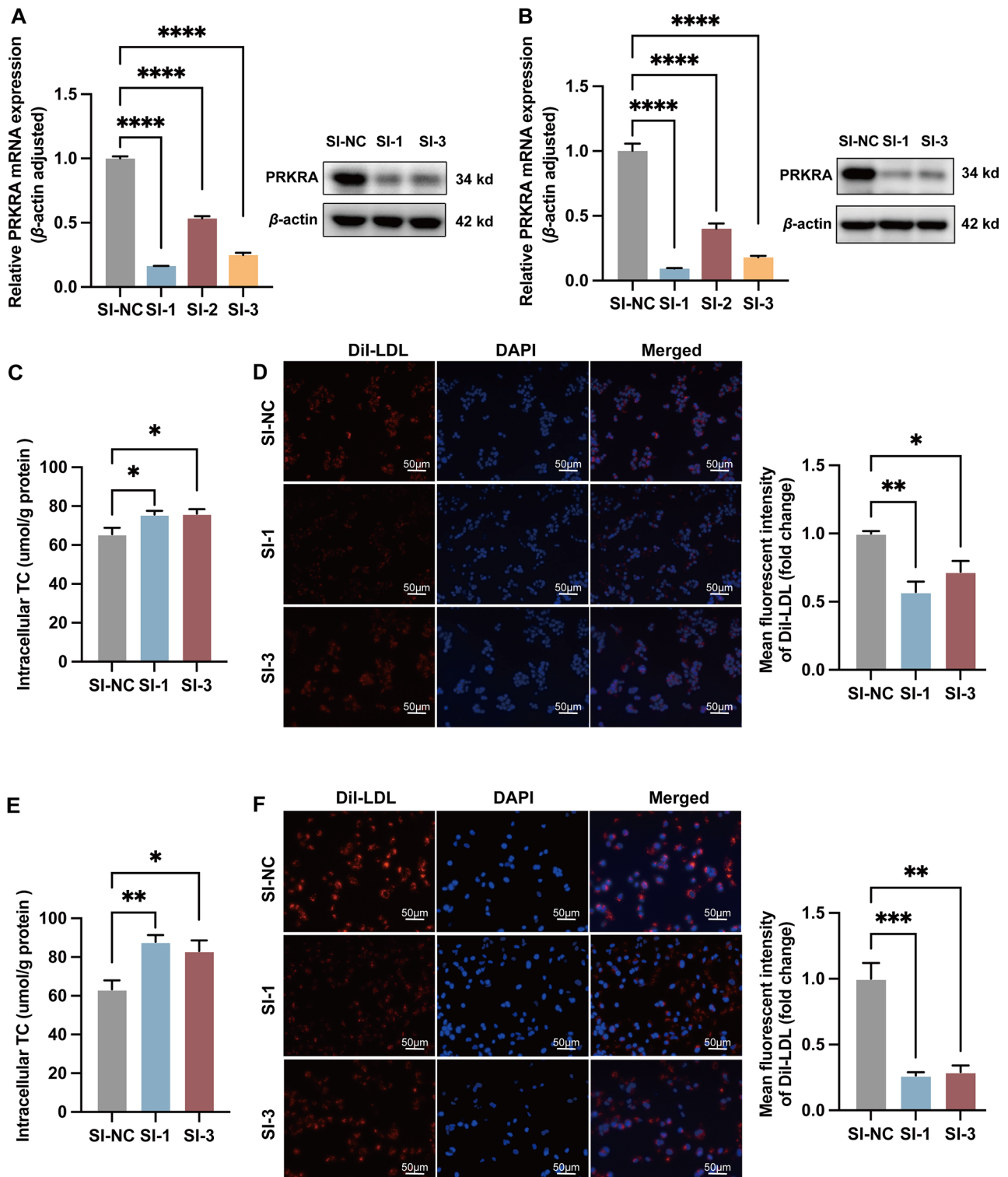


Fig. 4 PRKRA knockdown increased intracellular cholesterol accumulation and decreased LDL uptake. **(A)** PRKRA was successfully knocked down in HepG2 cells. **(B)** The efficiency of PRKRA knockdown in HuH7 cells. **(C)** Intracellular HepG2 cell cholesterol content. **(D)** DiI-LDL uptake in HepG2 cells and average fluorescence density analysis. **(E)** Intracellular cholesterol content of the HuH7 cell line. **(F)** DiI-LDL uptake in HuH7 cells and average fluorescence density analysis. Scale bar, 50 μm . The data are shown as the mean \pm SEM. Statistical significance is denoted as * $P < 0.05$, ** $P < 0.01$, *** $P < 0.001$, and **** $P < 0.0001$

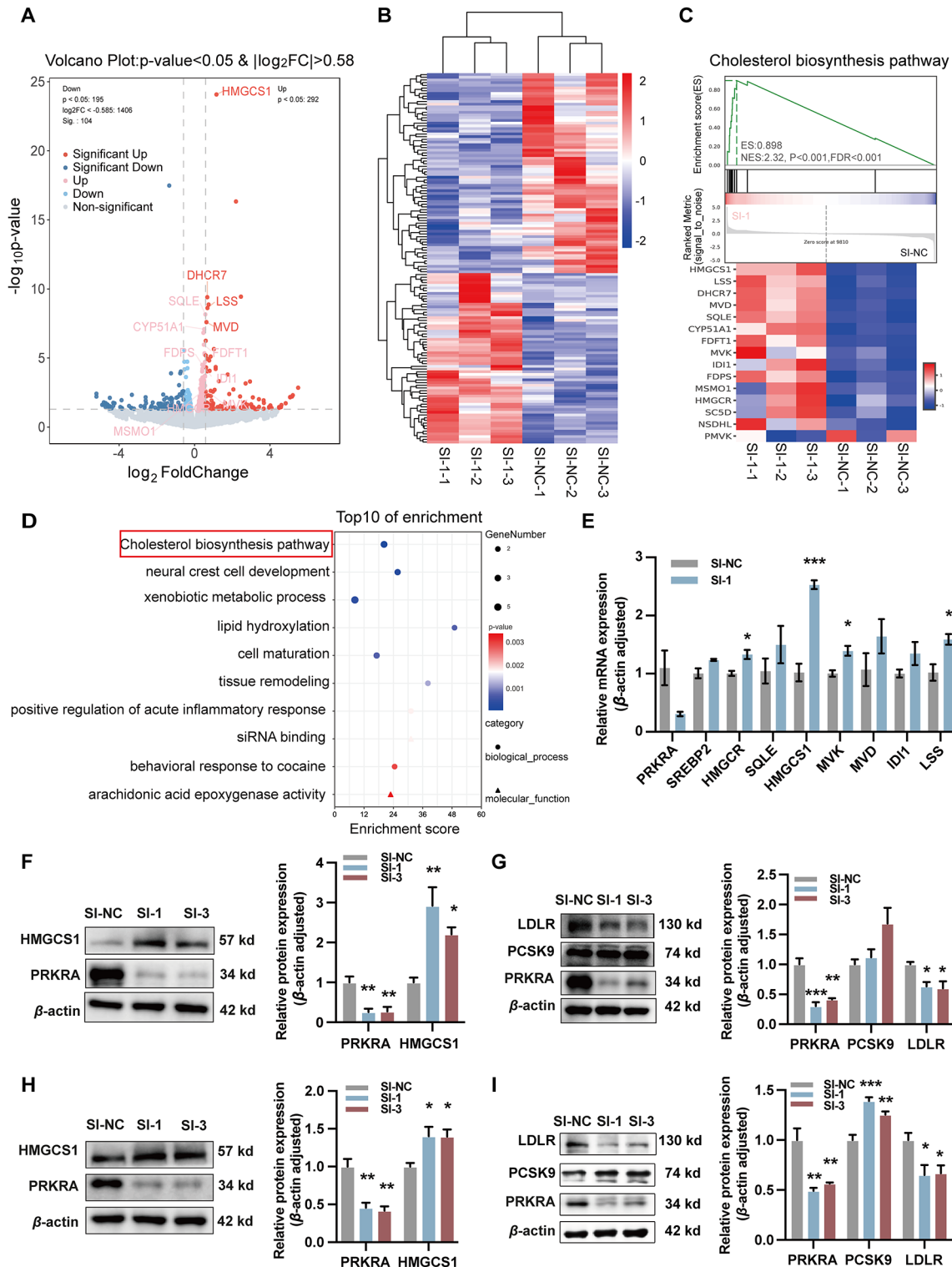


Fig. 5 Transcriptomic analysis revealed significant enrichment of the cholesterol synthesis pathway in PRKRA knockdown cells. **(A)** Differentially expressed genes in the si-NC vs. si-1 comparison in HepG2 cells. **(B)** A cluster heatmap displayed the gene expression profiles between si-NC and si-1 groups. **(C)** Gene set enrichment analysis demonstrated significant upregulation of the cholesterol biosynthesis pathway in the si-PRKRA group. **(D)** A bubble chart illustrating the results of the Gene Ontology and Kyoto Encyclopedia of Genes and Genomes pathway enrichment analyses demonstrating that the cholesterol biosynthesis pathway was enriched in the PRKRA knockdown group. **(E)** The mRNA levels of genes associated with cholesterol synthesis in HepG2 cells. **(F-G)** The protein levels of molecules associated with cholesterol synthesis and LDL uptake in HepG2 cells. **(H-I)** The protein levels of molecules associated with cholesterol metabolism in HuH7 cells. The data are shown as the mean \pm SEM. Statistical significance is denoted as $*P < 0.05$, $**P < 0.01$, and $***P < 0.001$; ns, not significant

results of the GO and KEGG pathway enrichment analyses indicated that the cholesterol biosynthesis pathway was enriched in the si-1 cohort (Fig. 5D). GSEA demonstrated a predominant enrichment of cholesterol biosynthesis pathway in the si-1 cohort (Fig. 5C). Cholesterol biosynthesis-related gene expression patterns were also observed in the two groups (Fig. 5C).

Building upon the transcriptome data, we employed qPCR analysis to validate the changes in the expression of crucial genes associated with cholesterol synthesis. QPCR results aligned with the transcriptomic findings (Fig. 5E). Additionally, we observed a significant increase in the protein expression of HMGCS1, a key enzyme in the cholesterol synthesis pathway, following PRKRA knockdown (Fig. 5F and H). Considering the alterations in LDL uptake capacity, we further examined the protein expression levels of PCSK9 and LDLR, two essential regulatory proteins involved in LDL uptake. The expression of LDLR was reduced in cells in which PRKRA was knocked down (Fig. 5G and I).

PRKRA overexpression decreased intracellular cholesterol levels and increased LDL uptake in hepatic cell lines

To further explore the regulation of cholesterol metabolism by PRKRA, we constructed a PRKRA-overexpressing cell line by transfecting HuH7 cells with a PRKRA-overexpressing lentivirus. Figure 6A and B indicate that PRKRA was successfully overexpressed in HuH7 cells.

Upon PRKRA overexpression, a reduction in the intracellular TC concentration and an increase in the LDL uptake capacity were observed in the HuH7 cells (Fig. 6C). At the molecular level, HMGCS1 protein levels were decreased in PRKRA-overexpressing cells and LDLR protein expression was increased (Fig. 6D). Additionally, the rescue experiment showed that after knocking down PRKRA with small interfering RNA in a stable HuH7 cell line overexpressing PRKRA, the regulatory effect of PRKRA on LDLR and HMGCS1 was restored (Fig. 6E).

Discussion

In this study, our findings revealed that the removal of ovaries for more than six months independently triggered an aberrant cholesterol metabolism phenotype in mice, and we observed a marked reduction in PRKRA expression in the liver tissue of the OVX mice. Furthermore, we found a correlation between decreased hepatic PRKRA mRNA expression and elevated serum total cholesterol levels associated with adverse menopause-related changes. Moreover, the expression of PRKRA could be regulated by E_2 and FSH in HepG2 and HuH7 cells. In addition, by manipulating PRKRA expression, we observed its essential involvement in hepatic cholesterol

metabolism, specifically in the regulation of cholesterol biosynthesis and LDL uptake, which are essential components of cholesterol homeostasis [28]. Furthermore, we demonstrated that PRKRA could regulate the expression of HMGCS1 and LDLR. These results indicated that PRKRA was involved in menopause-related cholesterol metabolism disorders. These findings might provide new insights for the treatment of these types of diseases.

Maintaining cholesterol homeostasis is vital for normal bodily function, and disruptions in this homeostasis are linked to numerous diseases that pose significant public health risks. Increasingly basic and clinical research results have indicated that menopausal status can affect cholesterol metabolism, with certain studies suggesting a greater susceptibility to dyslipidemia in postmenopausal women [29, 30]. However, the underlying mechanism behind this association remains unclear. Previous research has attributed this phenomenon to endocrine alterations, especially estrogen and FSH. However, some studies have shown that estrogen replacement therapy cannot fully ameliorate the dyslipidemia caused by ovariectomy in rats [31]. The side effects of hormone replacement therapy also limit its clinical application [32–34]. Therefore, it is vital to explore new therapeutic targets.

Our data revealed that ovariectomy could induce substantial alterations in both mouse liver and serum lipid profiles, consistent with the findings of prior investigations [35]. We observed decreases in PRKRA expression in liver tissue at both the mRNA and protein levels following ovariectomy. Furthermore, there was a negative correlation between PRKRA mRNA expression in the mouse liver and serum total cholesterol levels. Accumulating research has shown that fluctuations in E_2 and FSH levels are two important factors in the pathogenesis of menopause-related cholesterol metabolism disorders. Therefore, we detected whether estrogen or FSH affects PRKRA expression in HepG2 and HuH7 cells. The results showed that E_2 increased PRKRA expression, while FSH decreased it. Taken together, these findings and those of previous studies indicated the potential involvement of PRKRA in menopause-related cholesterol metabolism disruptions.

In the OVX mice, we observed increases in the serum TC and LDL-C levels. The elevated serum LDL-C levels may suggest a decrease in the ability of the liver to take up LDL from the bloodstream. Therefore, at the cellular level, in addition to assessing intracellular total cholesterol levels, we employed the Dil-LDL assay to evaluate the capacity of hepatocytes to internalize LDL from the culture medium, which indirectly reflects the ability of the liver to clear LDL-C from the blood. In vitro, our research revealed that knocking down PRKRA in HepG2 and HuH7 cells led to an increase in the total intracellular cholesterol level accompanied by a decrease in Dil-LDL

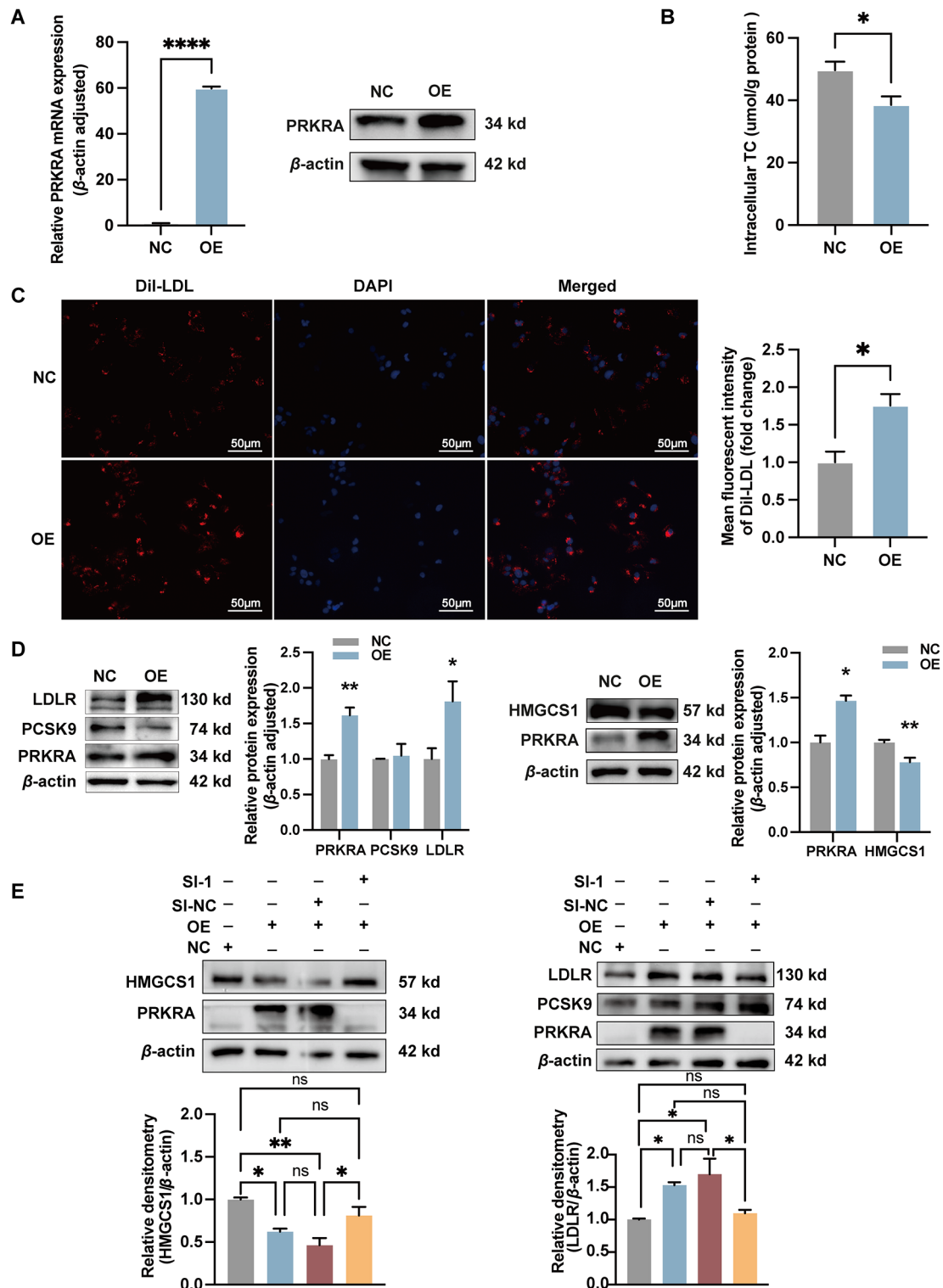


Fig. 6 PRKRA overexpression reduced intracellular TC levels and increased DiI-LDL uptake in HuH7 cells. **(A)** The level of PRKRA overexpression; **(B)** Decreased intracellular TC levels in PRKRA-overexpressing cells. **(C)** DiI-LDL uptake increased in the PRKRA-overexpressing cells. **(D)** PRKRA increased the protein expression of LDLR and decreased the protein expression of HMGCS1. **(E)** A rescue experiment was conducted to test the regulatory effect of PRKRA on HMGCS1 and LDLR. The histogram shows the mean \pm SEM of separate experiments for each group. Statistical significance is denoted as * $P < 0.05$, ** $P < 0.01$, *** $P < 0.001$, and **** $P < 0.0001$; ns, not significant

uptake. Conversely, when PRKRA was overexpressed, the intracellular TC level decreased, and this change was accompanied by an increase in Dil-LDL uptake.

To investigate the regulatory mechanisms of PRKRA in hepatic cholesterol metabolism, we employed transcriptomic analysis as a comprehensive approach. Given that basal PRKRA expression was greater in the HepG2 cell line than in the HuH7 cell line, we selected HepG2 cells with PRKRA knockdown for subsequent transcriptomic analysis. As highlighted in Fig. 5, transcriptomic analysis revealed significant upregulation of the cholesterol synthesis pathway in PRKRA-knockdown HepG2 cells. In this regard, we assessed the mRNA expression levels of key enzymes in the cholesterol synthesis pathway, including SREBP2, HMGCR, SQLE, HMGCS1, MVK, and MVD. Although the HMGCR expression measured in the transcriptome analysis, with a fold change of 1.28 and a *p*-value of 0.048, did not meet the criteria for differential expression (fold change ≥ 1.5 or < 0.5 , $p < 0.05$), we still investigated HMGCR expression because it serves as a rate-limiting enzyme in cholesterol synthesis. QPCR revealed an increase in HMGCR mRNA expression in cells with PRKRA knockdown; however, changes at the protein level were not detected in HuH7 cells (Supplementary Fig. 1). Based on the western blotting results, HMGCS1 levels significantly increased after PRKRA knockdown, which was consistent with the RNA sequencing results.

Due to changes in the ability of liver cells to uptake Dil-LDL, we also assessed the expression of LDLR, a transmembrane receptor responsible for LDL uptake [36]. The LDLR protein level decreased after PRKRA knockdown in both HepG2 and HuH7 cells. In contrast, PRKRA overexpression in HuH7 cells increased LDLR protein levels. PCSK9 is one of the crucial negatively regulated factors of LDLR [37]. We observed that PRKRA knockdown promoted PCSK9 expression in HuH7 cells, whereas no such effect was observed in HepG2 cells. Furthermore, LDLR, PCSK9, HMGCR, and other genes associated with cholesterol synthesis can be regulated by SREBP2. GSEA also revealed the upregulation of two SREBP2-related pathways, SREBF and miR33, in cholesterol and lipid homeostasis (WP2011) and sterol regulatory element-binding protein (SREBP) signaling (WP1982) in PRKRA-knockdown cells (Supplementary Fig. 2). However, after PRKRA knockdown, the changes in HMGCS1 and LDLR expression levels were not consistent. HMGCS1 expression increased, whereas LDLR expression decreased. This aspect warrants further exploration in our subsequent studies.

Despite the valuable insights gained, our study has certain limitations. First, due to constraints in experimental conditions, obtaining human liver samples to validate the changes in PRKRA protein levels was unfeasible.

Additionally, the absence of an estrogen replacement therapy group to evaluate whether PRKRA expression could be reconciled is another limitation. Furthermore, we did not validate the targeted therapeutic effect of PRKRA on the cholesterol metabolism disorders induced by OVX in mice. Nevertheless, this approach constitutes a priority for the subsequent phase of our research. In future studies, we will try to address these gaps comprehensively.

Conclusion

As mentioned above, the role of hormone replacement therapy is still controversial because of its adverse effects, such as the risk of breast cancer and venous thrombosis [38, 39]. Further experiments are warranted to explore the molecular therapeutic targets that may be involved in these disorders while also eliminating the side effects associated with hormone replacement therapy. Our study contributes incrementally to this ongoing exploration, providing valuable insight into potential strategies for alleviating menopause-related cholesterol metabolism disorders.

In conclusion, this study characterized a novel role of PRKRA and proposed for the first time that PRKRA is involved in menopause-related cholesterol metabolism. These findings offer a fresh perspective and may contribute to the development of innovative therapeutic strategies.

Abbreviations

PRKRA	Protein Activator of Interferon-Induced Protein Kinase
E2	17 β -Estradiol
FSH	Follicle-Stimulating Hormone
OVX	Ovariectomy
TC	Total Cholesterol
LDL	Low-Density Lipoprotein
LDL-C	Low-Density Lipoprotein Cholesterol
HDL-C	High-Density Lipoprotein Cholesterol
TG	Triglycerides
GEO	Gene Expression Omnibus
KEGG	Kyoto Encyclopedia of Genes and Genomes
GSEA	Gene Set Enrichment Analysis
SREBP2	Sterol Regulatory Element-Binding Protein 2
HMGCR	3-Hydroxy-3-Methylglutaryl-CoA Reductase
SQLE	Squalene Epoxidase
HMGCS1	3-Hydroxy-3-Methylglutaryl-CoA Synthase 1
LDLR	Low-Density Lipoprotein Receptor
PCSK9	Proprotein Convertase Subtilisin/Kexin Type 9
qPCR	Quantitative Polymerase Chain Reaction
WB	Western Blotting
CCK8	Cell Counting Kit-8

Supplementary Information

The online version contains supplementary material available at <https://doi.org/10.1186/s12944-025-02575-w>.

Supplementary Material 1

Supplementary Material 2

Supplementary Material 3

Acknowledgements

Not applicable.

Author contributions

L.X., Conceptualization; Data curation; Formal analysis; Investigation; Methodology; Project administration; Software; Validation; Visualization; Roles/Writing - original draft. J. X., Conceptualization; Formal analysis; Methodology; Software; Visualization; Roles/Writing - original draft. W.T.S., Conceptualization; Data curation; Formal analysis; Investigation; Methodology; S.Z., Investigation; Methodology. T.G., Conceptualization; Data curation; Resources; Supervision; Writing - review & editing; Project administration. S.E.Z., Conceptualization; Data curation; Funding acquisition; Resources; Supervision; Writing - review & editing; Project administration.

Funding

This research was supported by the Natural Science Foundation of China (81871132).

Data availability

The datasets used and/or analyzed during the current study are available from the corresponding author upon reasonable request.

Declarations

Ethical approval

All animal procedures performed in this study adhered strictly to both international and local ethical standards for animal research and have received approval from the Animal Welfare and Ethics Group, Department of Laboratory Animal Science, Fudan University (Approval ID: 2023110112).

Consent for publication

This manuscript has received unanimous approval from all the authors for publication.

Competing interests

The authors declare no competing interests.

Author details

¹Obstetrics and Gynecology Hospital of Fudan University, Number 149, Fangxie Road, Shanghai 200011, China

²Shanghai Key Laboratory of Female Reproductive Endocrine Related Diseases, Shanghai 200011, China

³Taian Maternity and Child Health Hospital, Taian, Shandong 271000, China

Received: 5 March 2024 / Accepted: 16 April 2025

Published online: 10 May 2025

References

- Harlow SD, Gass M, Hall JE, Lobo R, Maki P, Rebar RW, et al. Executive summary of the stages of reproductive aging Workshop + 10: addressing the unfinished agenda of staging reproductive aging. *J Clin Endocrinol Metab.* 2012;97:1159–68.
- Li H, Yu X-H, Ou X, Ouyang X-P, Tang C-K. Hepatic cholesterol transport and its role in non-alcoholic fatty liver disease and atherosclerosis. *Prog Lipid Res.* 2021;83:101109.
- Armeni A, Anagnostis P, Armeni E, Mili N, Goulis D, Lambrinoudaki I. Vasomotor symptoms and risk of cardiovascular disease in peri- and postmenopausal women: A systematic review and meta-analysis. *Maturitas.* 2023;171:13–20.
- Honigberg MC, Zekavat SM, Aragam K, Finneran P, Klarin D, Bhatt DL, et al. Association of premature natural and surgical menopause with incident cardiovascular disease. *JAMA.* 2019;322:2411–21.
- Robeva R, Mladenović D, Vesković M, Hrnčić D, Bjekić-Macut J, Stanojlović O, et al. The interplay between metabolic dysregulations and non-alcoholic fatty liver disease in women after menopause. *Maturitas.* 2021;151:22–30.
- Ko S-H, Kim H-S. Menopause-Associated lipid metabolic disorders and foods beneficial for postmenopausal women. *Nutrients.* 2020;12:202.
- Talaulikar V. Menopause transition: physiology and symptoms. *Best Pract Res Clin Obstet Gynaecol.* 2022;81:3–7.
- Rossouw JE, Anderson GL, Prentice RL, LaCroix AZ, Kooperberg C, Stefanick ML, et al. Risks and benefits of Estrogen plus progestin in healthy postmenopausal women: principal results from the women's health initiative randomized controlled trial. *JAMA.* 2002;288:321–33.
- Meng Y, Zong L. Estrogen stimulates SREBP2 expression in hepatic cell lines via an Estrogen response element in the SREBP2 promoter. *Cell Mol Biol Lett.* 2019;24:65.
- Y G, M Z, T B, S M, Z Y, W C, et al. Blocking FSH inhibits hepatic cholesterol biosynthesis and reduces serum cholesterol. *Cell research [Internet].* 2019 [cited 2023 Sep 19];29. Available from: <https://pubmed.ncbi.nlm.nih.gov/30559440/>
- Qiao S, Alamsi S, Wyatt A, Wartenberg P, Wang H, Candlish M, et al. Intra-pituitary follicle-stimulating hormone signaling regulates hepatic lipid metabolism in mice. *Nat Commun.* 2023;14:1098.
- Ou M-Y, Zhang H, Tan P-C, Zhou S-B, Li Q-F. Adipose tissue aging: mechanisms and therapeutic implications. *Cell Death Dis.* 2022;13:300.
- Stout MB, Justice JN, Nicklas BJ, Kirkland JL. Physiological aging: links among adipose tissue dysfunction, diabetes, and frailty. *Physiol (Bethesda).* 2017;32:9–19.
- Nelson HD. Menopause *Lancet.* 2008;371:760–70.
- Patel RC, Sen GC. PACT, is a protein activator of the interferon-induced protein kinase, PKR. *EMBO J.* 1998;17:4379–90.
- Patel CV, Handy I, Goldsmith T, Patel RC. PACT, a stress-modulated cellular activator of interferon-induced double-stranded RNA-activated protein kinase, PKR. *J Biol Chem.* 2000;275:37993–8.
- Chukwurah E, Farabaugh KT, Guan B-J, Ramakrishnan P, Hatzoglou M. A Tale of two proteins: PACT and PKR and their roles in inflammation. *FEBS J.* 2021;288:6365–91.
- Qiu J, Feng M, Yang G, Su D, Zhao F, Liu Y, et al. PRKRA promotes pancreatic cancer progression by upregulating MMP1 transcription via the NF-κB pathway. *Heliyon.* 2023;9:e17194.
- Hisamatsu T, McGuire M, Wu SY, Rupaimoole R, Pradeep S, Bayraktar E, et al. PRKRA/PACT expression promotes chemoresistance of mucinous ovarian Cancer. *Mol Cancer Ther.* 2019;18:162–72.
- Hennessy EJ, van Solingen C, Scacalossi KR, Ouimet M, Afonso MS, Prins J, et al. The long noncoding RNA CHROME regulates cholesterol homeostasis in primates. *Nat Metab.* 2019;1:98–110.
- Liu DJ, Peloso GM, Yu H, Butterworth AS, Wang X, Mahajan A, et al. Exome-wide association study of plasma lipids in > 300,000 individuals. *Nat Genet.* 2017;49:1758–66.
- Yi J, Hu H, Shi P, Shi S, Zhao J, Xu L, et al. Differential analysis of quantitative proteome and acetyl-proteome profiling between premenopausal and postmenopausal ovarian tissues. *Clin Proteom.* 2018;15:36.
- Nigro M, Santos AT, Barthel CS, Louzada RAN, Fortunato RS, Ketzler LA, et al. A change in liver metabolism but not in brown adipose tissue thermogenesis is an early event in ovariectomy-induced obesity in rats. *Endocrinology.* 2014;155:2881–91.
- Malinská H, Hüttl M, Miklánková D, Trnovská J, Zapletalová I, Poruba M, et al. Ovariectomy-Induced hepatic lipid and cytochrome P450 dysmetabolism precedes serum dyslipidemia. *Int J Mol Sci.* 2021;22:4527.
- Xu XD, Chen J, Ren J. Experiment of Low-density lipoprotein absorption. *Bio-101.* 2021;e1010831.
- Fu W, Gao X-P, Zhang S, Dai Y-P, Zou W-J, Yue L-M. 17β-Estradiol inhibits PCSK9-Mediated LDLR degradation through GPER/PLC activation in HepG2 cells. *Front Endocrinol (Lausanne).* 2020;10:930.
- Kelly LA, Seidlova-Wuttke D, Wuttke W, O'Leary JJ, Norris LA. Estrogen receptor alpha augments changes in hemostatic gene expression in HepG2 cells treated with estradiol and phytoestrogens. *Phytomedicine.* 2014;21:155–8.
- Luo J, Yang H, Song B-L. Mechanisms and regulation of cholesterol homeostasis. *Nat Rev Mol Cell Biol.* 2020;21:225–45.
- Zhao D, Guallar E, Ouyang P, Subramanya V, Vaidya D, Ndumele CE, et al. Endogenous sex hormones and incident cardiovascular disease in Post-Menopausal women. *J Am Coll Cardiol.* 2018;71:2555–66.
- Nappi RE, Chedraui P, Lambrinoudaki I, Simoncini T. Menopause: a cardiovascular metabolic transition. *Lancet Diabetes Endocrinol.* 2022;10:442–56.
- Boldarine VT, Joyce E, Pedrosa AP, Telles MM, Oyama LM, Bueno AA, et al. Oestrogen replacement fails to fully revert ovariectomy-induced changes in adipose tissue monoglycerides, diglycerides and cholesteryl esters of rats fed a lard-enriched diet. *Sci Rep.* 2021;11:3841.
- Vinogradova Y, Coupland C, Hippisley-Cox J. Use of hormone replacement therapy and risk of venous thromboembolism: nested case-control studies using the QResearch and CPRD databases. *BMJ.* 2019;364:k4810.

33. Vinogradova Y, Denning T, Hippisley-Cox J, Taylor L, Moore M, Coupland C. Use of menopausal hormone therapy and risk of dementia: nested case-control studies using QResearch and CPRD databases. *BMJ*. 2021;374:n2182.
34. Vinogradova Y, Coupland C, Hippisley-Cox J. Use of hormone replacement therapy and risk of breast cancer: nested case-control studies using the QResearch and CPRD databases. *BMJ*. 2020;371:m3873.
35. Buniam J, Chukijrungsat N, Khamphaya T, Weerachayaphorn J, Saengsirisan V. Estrogen and voluntary exercise attenuate cardiometabolic syndrome and hepatic steatosis in ovariectomized rats fed a high-fat high-fructose diet. *Am J Physiol Endocrinol Metab*. 2019;316:E908–21.
36. Defesche JC, Gidding SS, Harada-Shiba M, Hegele RA, Santos RD, Wierzbicki AS. Familial hypercholesterolaemia. *Nat Rev Dis Primers*. 2017;3:17093.
37. Seidah NG, Prat A. The multifaceted biology of PCSK9. *Endocr Rev*. 2022;43:558–82.
38. Lobo RA. Hormone-replacement therapy: current thinking. *Nat Rev Endocrinol*. 2017;13:220–31.
39. Flores VA, Pal L, Manson JE. Hormone therapy in menopause: concepts, controversies, and approach to treatment. *Endocr Rev*. 2021;42:720–52.

Publisher's note

Springer Nature remains neutral with regard to jurisdictional claims in published maps and institutional affiliations.